Flow Structure of the Solids in a 3-D Gas–Liquid–Solid Fluidized Bed

F. Larachi, M. Cassanello, J. Chaouki, and C. Guy
Dept. of Chemical Engineering, École Polytechnique, Montréal, Québec, Canada H3C 3A7

Local and macroscopic solids flow structure and kinematics in a 3-D gas–liquid–solid fluidized bed were studied using a noninvasive radioactive-particle tracking (RPT) technique. Based on the multisite detection of γ radiations emitted from a single radiolabeled tracer particle freely moving in the fluidized bed, RPT permitted to obtain fast sampling of 3-D trajectories of the tracer, whose physical properties were similar to those of the solids inventory. These trajectories showed the detailed motion sequences of the solid particles as entrained in the bubble wakes, fluctuating randomly or sinking deterministically in the liquid–solid emulsion. Based on measurements done in the vortical-spiral flow regime, the dynamic solids flow structure inside a three-phase fluidized bed can be viewed as a three-zone core–annulus–annulus structure: (1) a central fast-bubble flow region with the particles swirling upward; (2) a vortical flow region around the velocity inversion point with the particles momentarily captured in emulsion vortices; and (3) a relatively bubble-free descending flow region where the particles spiral down between the velocity inversion point and vessel walls. Our solids flow structure of dense fluidized beds are similar to the flow structure of liquid and/or solid in lean fluidized beds (observed through laser sheeting imaging). Measured distributions of local ensemble-averaged particle velocities and turbulence intensities were consistent with the existence of a toroidal recirculatory solids flow pattern in the bed. Measured mean circumferential ensemble-averaged radial velocity was essentially zero throughout most of the bed. The solids flow turbulence field was nonisotropic, as radial turbulence intensities were generally lower than longitudinal turbulence intensities.

Introduction

Gas–liquid–solid fluidized systems have made inroads into a variety of industrial applications that extend nowadays from heavy oil, petroleum resid, and synthetic crude processing to fermentation and aerobic biological wastewater treatment. In spite of their importance, and despite huge efforts made both experimentally and theoretically to unveil the mechanisms of the intimately intermingled three-phase flow patterns, a satisfactory comprehension of three-phase fluidization is still lacking. This was partly due to the absence of reliable data and of highly resolved (in space and/or in time) measuring techniques capable of capturing the inherent complexity in the flow. A complexity that is reflected by the seemingly erratic local fluctuations of phase holdups and velocities, by the inception of gross circulation flow patterns or "gulf stream," or by the interaction between bubbles and liquid and/or solids via wake phenomena. Without the formulation of new flow concepts interpreting and of new models integrating such a complexity, any attempt at understanding and scaling up three-phase fluidized beds would be incomplete and doomed to fail.

Very little is known about the flow structure of solids in gas–liquid–solid fluidized beds. The motion of the solids phase in these reactors has not been extensively studied, and data on the undisturbed *in situ* solid-particle movements and models to describe them are almost nonexistent. Most of the

Correspondence concerning this article should be addressed to J. Chaouki.
New address of: F. Larachi, Dept. of Chemical Engineering, Laval University, Sainte-Foy, P.Q., Canada G1K 7P4; M. Cassanello, PINMATE, Dept. de Industries, FCEyN, Universidad de Buenos Aires, 1428 Ciudad Universitaria, Buenos Aires, Argentina.

previous studies overwhelmingly focused on bubble-induced liquid flow in bubble columns (Hills, 1974; Franz et al., 1984; Devanathan et al., 1990; Dudukovič et al., 1991; Chen et al., 1994; Reese and Fan, 1994) and gas–liquid–solid fluidized beds with low solids content (10% and down, Chen and Fan, 1992; Tzeng et al., 1993; Chen et al., 1994). In the latter case, the slurry mixture is viewed as an individual phase, to which the general flow regimes and macroscopic flow structures are qualitatively similar to those of a bubble column. A gross circulation flow pattern has been observed for these systems, in which the liquid or the liquid–solid mixture flows upward in the core region of the column and downward in the sidewalls. The occurrence of the gross liquid (or liquid–solid) circulation was attributed to large bubbles or bubble clusters preferentially evolving in the central core of the column. Similar gross circulation patterns have also been reported for the solids in gas fluidized beds (Lin et al., 1985; Moslemian et al., 1989) and three-phase fluidized beds containing binary mixtures of solids (Larachi et al., 1995). Quantitatively, the gross circulation pattern has been characterized by means of time or ensemble-averaged velocities averaged within finite voxels in which the flow field is compartmentalized. However, it became clear that long-time averaged flow patterns do not reflect the flow instantaneous patterns, as unsteady coherent structures in the flow are generally overlooked in the averaging procedure. A direct consequence of this is the impossibility of predicting time-averaged flow patterns from steady-state models since the long-time integrals over flow fluctuations do not vanish but lead to additional terms that, at present, cannot be successfully approximated for multiphase flows (Sokolichin and Eigenberger, 1994). Therefore, the development and the application of dynamic models is of essential importance for a better understanding of the basic phenomena present in three-phase fluidized beds. Moreover, assessment of these models is possible only if the true instantaneous flow phenomena can be experimentally quantified.

It appears that the first investigation that shed light on the existence of instationary three-dimensional coherent flow structures of liquid or slurry mixture in three-phase systems was due to Fan et al. (1992). Later, Fan's team (Tzeng et al., 1993; Chen et al., 1994), by means of laser sheeting and particle image velocimetry (PIV) techniques in 2-D and 3-D beds, set up, for the vortical-spiral flow regime where the gross circulation pattern occurred, a four-zone flow structure model consisting of (1) a sidewall descending flow region, (2) a vortical–spiral region, (3) a fast bubble-flow region, and (4) a central plume region. This central plume region was indistinguishable in small-diameter columns due to the mergence with the fast-bubble flow region (Chen et al., 1994). These authors suggested that in the conventional coalesced bubble flow regime, two subregimes are distinguishable, namely a vortical-spiral flow regime at lower gas velocity and turbulent flow at high gas velocity. They characterized the vortical-spiral flow regime as a transition regime between the dispersed regime and turbulent flow. Refractive index mismatch between the liquid and the solid phases restricted observation of the flow structure with the laser flow visualization technique to below 10% solids holdup conditions (Chen et al., 1994). Thorough qualitative and quantitative information was given for the liquid phase, whereas the solids-base behavior was reported only qualitatively. The previously mentioned

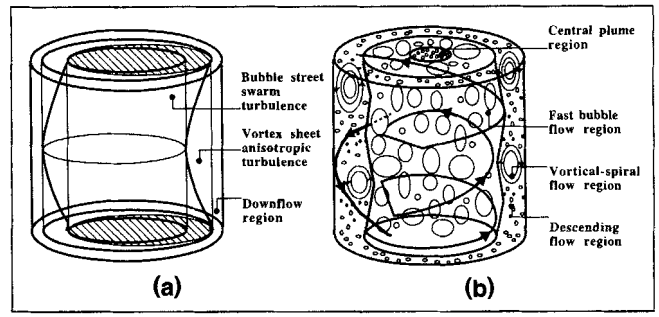

Figure 1. Flow structure in the vortical-spiral flow regime in a 3-D (a) gas–liquid bubble column (Franz et al., 1984) and (b) gas–liquid–solid fluidized bed and bubble column (Chen et al., 1994).

conceptual flow structure proposed for the bulk region has been built up from significant work by Franz et al. (1984) on the liquid flow structure in bubble columns. Using a hot-film anemometry technique, Franz et al. (1984) measured for the liquid time-averaged Eulerian velocity and root-mean-square velocity profiles in the azimuthal, radial, and axial directions. They proposed that the bubbly two-phase flow be divided into three instantaneous zones: (1) a central bubble street with swarm turbulence and helical bubble flow; (2) a vortex sheet of anisotropic turbulence; and (3) a sidewall downflow region. Figure 1 sketches the two conceptual instantaneous flow structures proposed by Franz et al. (1984) and by Chen et al. (1994). Both models agree that in the central fast-bubble flow region, the liquid rises in a spiral or helical manner.

As was shown by the preceding literature review, there is still a lack of experimental data on the dynamic behavior and flow structure of the solids phase in gas–liquid–solid fluidization under more realistic conditions of column geometry and solids holdup. In this work, experiments are conducted in a 3-D column to explore the dynamic behavior of the solids at holdups typical of a three-phase fluidized bed, and to compare the results obtained to those observed by Chen et al. (1994) for low solids holdup in dilute fluidized beds (10% solids and down). Noninvasive radioactive particle tracking (RPT) was chosen as a method to develop the detailed solids flow information needed. RPT is capable of providing fast-sampled instantaneous coordinates $[x(t), y(t), z(t)]$ of a wandering tracer particle, whose size and density aptly mimic those of the bed inventory, over very long periods of observation (up to 15 h). Then the coordinates of the tracer are converted into local and instantaneous velocity components from successive differentiations of the points on the trajectory. It is important to mention that RPT is a position-sensitive technique that primarily measures instantaneous coordinates x, y, and z, and not velocity components as most velocimetric techniques do. Moreover, RPT is a Lagrangian measuring technique that provides instantaneous and pointwise flow information, and as such it should be distinguished from the existing flow-visualization techniques, such as PIV, which are essentially Eulerian techniques capable of providing full-field instantaneous and average-velocity profiles. With these techniques, owing to the presence of many seeds in the flow, full-field information is derived from sensing sheets through

the flow a few cm^2 in extent (e.g., laser sheeting); whereas RPT, with its individual tracer, only provides ensemble-averaged flow information over the whole field after collection of a representative amount of flow data.

Given accurate knowledge of the particle movements, a wealth of transient and steady-state information on the solids phase can be inferred. Thus, RPT data are utilized for (1) quantification of the solids flow structure and solids motion mechanisms; (2) obtaining bubble-wake and solids-offset flow-velocity distributions; (3) evaluating solids mixing times in the three directions of space; (4) mapping the averaged full flow-field velocity vectors and turbulence fields. Other informations, such as turbulence coefficient fields, Lagrangian auto/cross-correlations and macroscale times, circulation time distributions, and particle behavior in the entrance region or in the disengagement zone, can also be derived.

Experimental Studies

Particle of tracking

Noninvasive tracking of individual radioactive particles freely moving in multiphase equipment had proved to be a very reliable technique for investigation of the solids or the liquid dynamics in many reactors, such as gas fluidized beds (Lin et al., 1985; Moslemian et al., 1989) or bubble columns (Devanathan et al., 1990; Dudukovič et al., 1991; Moslemian et al., 1992; Dudukovič and Devanathan, 1993; Yang et al., 1992, 1993). The work on RPT at École Polytechnique was initiated by Chaouki's team to develop a tracking system similar to those pioneered by the preceding researchers, but more accurate with respect to particle locations, owing to improved inverse reconstruction algorithms (Larachi et al. 1994), and by finding unprecedented applications of the tracking system to other two- or three-phase reactor types of interest for the industry.

The particle tracking system consists of eight 76 mm × 76 mm uncollimated and unshielded NaI(Tl) scintillation detectors mounted around the reactor to be studied (see Figure 2). The movement of a γ-ray emitting tracer, made of ^{46}Sc radionuclide, with a diameter and a density similar to that of the glass beads used as the bed particles, is followed by the detectors, which continuously and simultaneously measure count rates for several hours. Different amounts of γ-rays impinge on each detector, depending on the tracer location in the bed, the corresponding subtended effective solid angle, and the bed attenuation. Taking advantage of detector redundancy, the γ-ray counts are interpreted by a triangulation technique to yield the instantaneous particle position. To accurately evaluate the attenuation of γ-rays in the bed, a calibration is repeated for each experiment when at least one operating condition is changed. Further details on the tracking technique can be found in Larachi et al. (1994).

Experimental setup

The results presented in this work were obtained in a Plexiglas column of 100 mm inner diameter and a height of 1,500 mm. The solids inventory made of 3-mm glass beads (density = 2,475 kg/m^3) was fluidized with a cocurrent upward air–water flow at ambient temperature and atmospheric

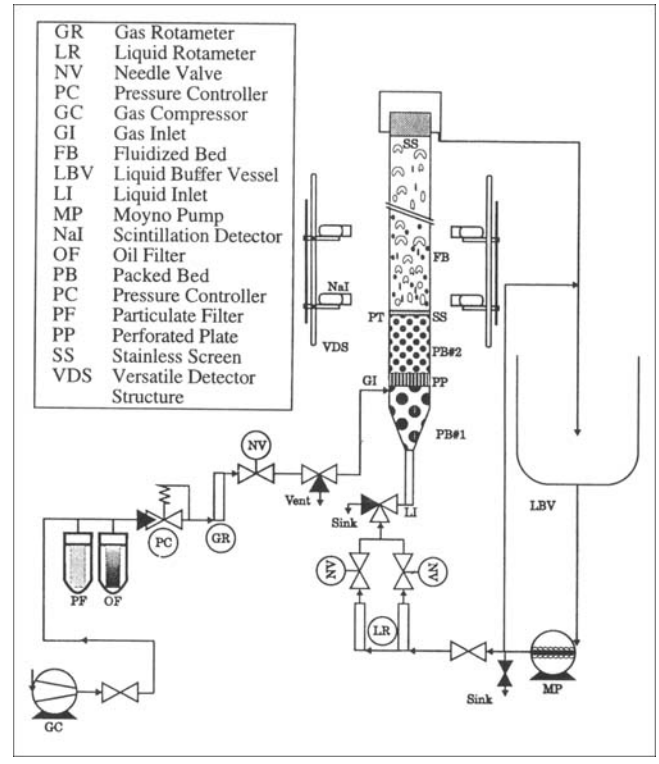

Figure 2. Experimental arrangement of the three-phase fluidized bed.

pressure. The superficial gas velocity was varied between 0.032 and 0.106 m/s, while the superficial liquid velocity was maintained constant at 0.065 m/s. Both the dispersed and the coalesced bubble flow regimes were observed within these conditions. Throughout this article, only the particles' behavior in the coalesced bubble flow regime are described in detail. The remaining experiments conducted in the dispersed bubble flow regime (gas velocity < 0.069 m/s) showed behaviors qualitatively similar to those of fluidization of binary mixtures of solids for the same flow regime (Larachi et al., 1995) and are not shown here.

The experimental setup is shown in Figure 2. The column was fitted with a three-stage gas–liquid distributor comprising a conical-base packed bed 150-mm high containing 5-mm glass beads that acted as a liquid calming zone, and a sandwiched 3-mm-thick perforated plate topped by a 200-mm-high cylindrical packed bed containing 2-mm glass beads. Fine mesh screens were provided at each side of the column to circumvent entrainment of the fluidized particles or their contact with the distributor particles. Air was fed to the bed through three horizontal 6.35 mm tube injectors. The injectors, with 120° spacing, were capped by stainless steel cups (pore size = 20 μm) and placed immediately beneath the perforated plate (5.5% open area with 0.74-mm holes arranged in a 2-mm triangular pitch). To ensure uniform air injection in the column, air flow rates through the injectors were individually adjusted by needle valves. Air-pressure drop was kept around 190 kPa upstream of the tube injectors. Liquid supply was ensured by a Moyno pump. Fluid throughputs, controlled by rotameters, and solids inventory were set so as to maintain expanded three-phase emulsion levels be-

tween 450 and 650 mm above the distributor (aspect ratios = 4.5 to 6.5). On top of the column, an overflow system separated the gas from the liquid. Water was recycled into a 100-L buffer vessel, and air was vented to the atmosphere.

Prior to each experiment, the bed was fluidized and a set of measurements of γ-ray count rates was made to calibrate the system using the radioactive tracer particle rigidly positioned at 150 representative and known locations in the bed. Then the tracer was dropped into the column and, after several minutes of fluidization, the particle tracking was started. Data collection and acquisition typically continue for 7 h with photon count rates acquired synchronously every 30 ms by all the scintillation detectors. Data processing for the recovery of the tracer coordinates at each instant of time from the redundant γ-ray count rates was performed off-line on an IBM 375 RISC 6000 workstation computer.

Results and Discussion

Solids kinematics

The discussion hereafter on the particle instantaneous movements will be subdivided into five parts as follows: wake phenomena, particle upward movement, particle downward movement, vortical flow region, and particle rising and descending velocities.

Wake Phenomena. The instantaneous displacements of the 3-mm tracer in the z direction (vertical coordinate parallel to column axis) are examined first. Figure 3a illustrates a chart depicting 60 s of successive axial coordinates of the tracer particle (only 2,000 sample points from about 1 million points). Motion is observed along the length of the bed with the positions bounded by the distributor and the disengagement zone, which both confine the tracer movements between $z = 0$ and $z \approx 650$ mm, that is, the highest altitude attainable by the particles. Clearly, the particle motion displays recursive convective patterns whereon small-amplitude and high-frequency random fluctuations are superimposed. Zooming in the ascending (ζ_1) and descending (ζ_4) portions of the particle vertical movements shows that the displacements are carried out at almost constant axial velocities dz/dt ($dz/dt = 408$ mm/s for ζ_1 and $dz/dt = -419$ mm/s for ζ_4), as is demonstrated, for example, by the best linear fits of the z vs. t curves shown in Figure 3b. A pair of successive rising and descending portions form unsymmetrical peaks that show sharp ascent and descent of different lengths (Figure 3a). These large-amplitude vertical movements can be either smooth or jittery, and may sometimes extend uninterruptedly from the distributor to the freeboard region. Moreover, most of the random fluctuations on the vertical displacements occur when the particle peaks at a maximum height or dives to a minimum height (see Figure 3a). Though these maxima and minima take place along the entire bed height, they appear to concentrate more in the upper part.

Kitano and Fan (1988) and Kreischer et al. (1990), in studying the wake dynamics of solitary bubbles in 2-D and 3-D liquid fluidized beds, probed the bubble wake structure and quantitatively showed that bubble wakes can carry up solids of submillimetric size. Although the solid particles generally move upward due to both the primary wake capture and the drift effect, the latter is insignificant for high-density particles, as pointed out by Miyahara et al. (1989) and

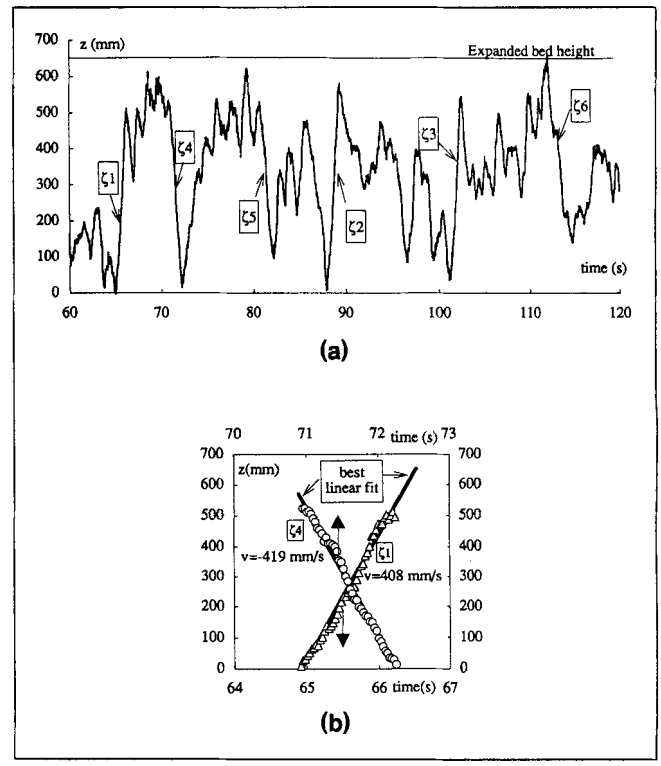

Figure 3. (a) Displacement-time chart showing the variation in axial position of the tracer over 60 s; (b) a zoom of a rising (ζ_1) and a descending (ζ_4) portion from the vertical movement together with the best regression lines and the corresponding slopes (or velocities).

Tsuchiya et al. (1992). The large-amplitude vertical movements observed in this study (Figure 3a) clearly play an influential role in the solids mixing process of a three-phase fluidized bed. The 3-mm tracer particle travels upward and downward very quickly (see for example trajectories ζ_1 to ζ_6 of Figure 3a), and its trajectory quite often covers the whole height of the bed. The only explanation for such a movement is that the particle is kept within the wake region of past ascending bubbles (trajectories ζ_1–ζ_3, Figure 3a). As a response to the depletion in solids for some regions of the bed due to bubble-wake transport, a spontaneous and simultaneous compensating and descending offset flow is provoked (trajectories ζ_4–ζ_6, Figure 3a). The results of this study are the first demonstrated of large and heavy particles moved up by bubble wakes in realistic conditions of a multibubble fluidized bed. For example, Figure 3a should be a warning of how miscounting could be the assumption of a solid-free wake in a gas–liquid–solid fluidized bed containing large inertia particles such as 3-mm glass beads.

The fact that the rising history of particles likely matches that of wake-generating bubbles confirms the complex structure of bubble wakes. RPT shows the existence of two regions in the wake; a stable solids region driven by the leading bubble and traveling at the same velocity (rising portions, Figure 3a), and a shedding wake region (maximums, Figure 3a) from which particles are expelled toward the liquid–solid

emulsion. A dynamic exchange process existing between these two zones allows the shedding region to collect particles from the stable region. Particles are thus allowed to be discharged in the emulsion almost everywhere along the bed height (see the maximums in Figure 3a). A careful look at the rising lines pictured in Figure 3a reveals that they are not always smooth, but exhibit jitters with slope changes at some places. At those places bubble–bubble interactions likely occur, leading to faster coalesced bubbles (steeper slope), slower broken up bubbles (lower slope), or bubbles accelerated by other bubbles closely spaced in front (Miyahara et al., 1991). The two aforementioned wake regions for a multibubble fluidized bed share certain similarities with far more complex primary-wake structures, as was observed by Kitano and Fan (1988), Kreischer et al. (1990), and Tsuchiya and Fan (1988) during injections of solitary bubbles in 2-D and 3-D fluidized beds.

Now it becomes clear that each time the particle vertical coordinate reaches a maximum and goes down right after a wake containing the tracer particle is shed off from the parent bubble. Although particles might be expelled from the wakes sooner due to the turbulent wake flow, it is presumed that solids essentially exchange in one piece by a cyclic shedding process (Tsuchiya and Fan, 1988). Consequently, an axial wake-shedding distribution or a wake-emulsion solids exchange distribution can be approached from the number of times the tracer particle reaches a maximum in a z vs. time chart. The probability $W(z)$ that a particle is shed off from a wake between levels z and $z+\Delta z$ can be computed as $W(z)\cdot\Delta z = \Delta N(z)/N_0$, where $\Delta N(z)$ is the number of maximums counted between z and $z+\Delta z$, and N_0 is the total number of maximums counted for the whole run. Figure 4 shows the obtained wake shedding distribution. It is seen that wakes nonuniformly exchange solids with the liquid–solid emulsion all along the bed height. This exchange becomes more intense as one moves away from the distributor region. The nonisolated nature of the solids contained in the wakes is also confirmed (Fan, 1989). $W(z)$ increases progressively with axial position until 450 mm, after which the number of sheddings suddenly rises and from 550 mm, it falls sharply near the disengagement zone. By evaluating the area under the curve, it is found that half of the wake sheddings occur in the upper third of the bed.

In an attempt at modeling the longitudinal mixing characteristics of the solids in three-phase fluidized beds, the authors developed a one-dimensional, two-zone model that postulates that axial mixing is determined by the action of primary wakes and a wake-emulsion mass transfer (Cassanello et al., 1996). The former are responsible for the convective upward motion of the solid (ascending portions in Figure 3a), and the latter allow the compensating downward motion to take place in the emulsion phase (descending portions in Figure 3a). Using only this knowledge of the particle velocities (see below for their determination), the model was successful in predicting the measured longitudinal mixing times, as well as in describing the dynamics of the spread of particle clouds. In another article, the authors analyzed the times series such as those shown in Figure 3a using a frame of deterministic chaos (Cassanello et al., 1995) and found that the solids dynamics in three-phase fluidization is chaotic. Since a chaotic behavior can only arise from nonlinear dynamics, mathematical models that aim at describing the solids motion in these

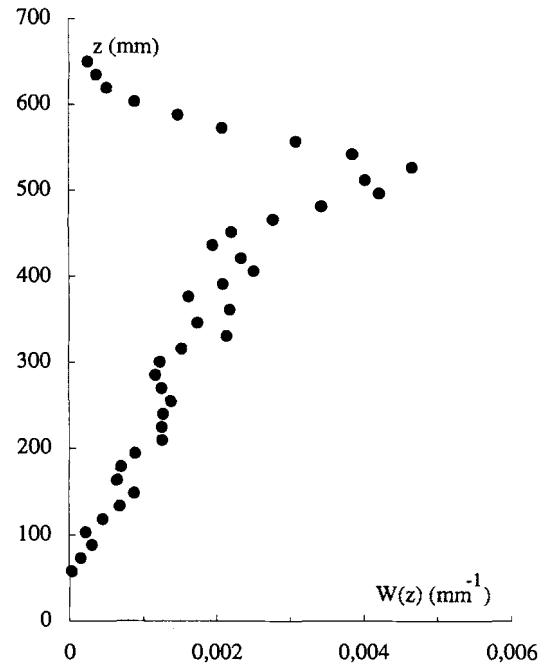

Figure 4. Wake–emulsion exchange density function of the solids in the axial direction.

systems should contain a minimum of linear complexity. Calculation of the correlation dimensions of the tracer trajectory time series in the vortical-spiral flow regime showed values as high as 15, indicating that in this regime the number of variables needed to describe the solids-phase dynamics in three-phase fluidization is relatively high.

Particle Upward Movement. Let us now go further in breaking down the particle rising movements into their elementary parts. Figure 5a shows r vs. z instantaneous motions of the tracer for the three ascending paths, ζ_1, ζ_2, and ζ_3 in Figure 3a. Long-range paths have voluntarily been chosen because they are believed to display more complete features of the elementary steps involved in the solids motion. Recall that the time elapsed between two successive positions is 0.03 s. Figure 5b shows projected instantaneous displacements of the tracer on plane xy for path ζ_2. The arrowed smooth line drawn on Figure 5b is here to facilitate tracking down the horizontal course of the trajectory. The ellipse enclosing the horizontal projection is calculated assuming (1) a major axis a given by the maximum horizontal distance separating the two farthest points on the rising trajectory, and (2) a minor axis b given by the maximum horizontal distance of the points projected perpendicularly to the major axis. The ellipse, represented by the outermost closed contour, gives the total horizontal area expected to be covered by the rising bubble wake containing the tracer particle. Even though more complicated contours can be used, elliptical shapes have been elected only for convenience. After defining proper boundaries based on solids rising movements, delimitation of the region of flow where bubble wakes are active can be determined.

From Figure 5a, it is seen that near the distributor, particles are either carried up inward to the center (ζ_2 and ζ_3) or entrained in a small loop (ζ_1) before being successively expelled outward to the wall by the spouting gas and redirected

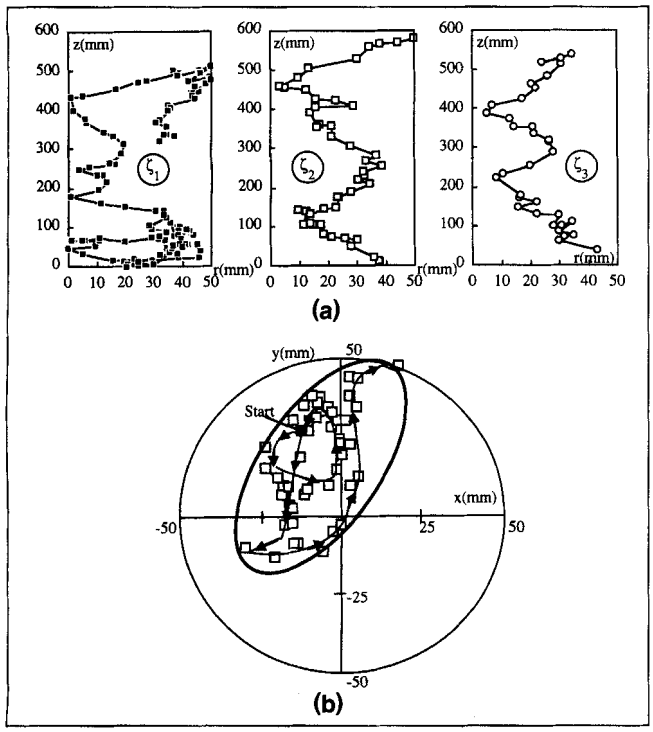

Figure 5. Typical features exhibited during particle ascents (a) radial vs. axial displacements for the rising portions ζ_1, ζ_2, and ζ_3, and (b) cross-sectional movements for ζ_2.

back toward the center in a rising motion. Then these particles pursue rising with a zigzag secondary motion until they reach the freeboard. Recall that not all the particles are discharged in the disengagement zone as Figure 4 pictured it. The zigzag secondary motion observed in Figure 5a probably arises from alternate sheddings of vortices from the bubble wakes (Fan, 1989) or from dynamic directional changes due to multiple bubble streams interacting simultaneously. In addition, whenever their ascent is interrupted, the particles are subjected to a radial outward flow (Figure 5a). This occurs predominantly in the sidewall region. There, the particles are momentarily shut up in sidewall vortices, and then sink diagonally inward with a spiraling movement until they meet another rising bubble wake and initiate a new ascent (see below for a detailed description of the descending movement). It is within these vortices that the particles exhibit the random longitudinal fluctuation pattern of the maximums seen in Figure 3a. Similar zigzag tracks, sidewall discharge, and vortices are also seen in the case where the particle is shed off in the three-phase emulsion far beneath the freeboard.

Aided by top views of the trajectories, the three-dimensional nature of the ascending paths is shown in Figure 5b. Particles execute swirling movements of very irregular loops and spiral pitch. The central loci of these 3-D spirals do not form straight vertical lines and allow a third elementary movement, namely a rocking movement, to be identified. Sometimes, flat curls are observed on the same spiraling ascent, revealing interference with two-dimensional swinging movements. The elementary particle movements identified in this work coincide very well with recent observations made by Chen et al. (1994) on the bubbles, liquid, and solids motions in the vortical-spiral flow regime of low solids holdup fluidized beds (less than 10% solids). According to their observations, clusters of bubbles or coalesced bubbles move upward in a spiral/rocking manner and, with a similar movement, carry up both the particles and the liquid phase. The striking similarities in the motion behaviors observed from both studies indicate that the solids rise in a bubblelike motion and are submitted to the same qualitative kinematic mechanisms.

Let us now delineate the boundaries of the region where the particles preferentially rise in the bed. Figure 6a is a plot of the distributions of the major a and minor b axes of the ellipses enclosing the horizontal projections of the rising particle paths for the whole experiment. There is a wide variation in the length of both axes, as well as in the shape of the distributions. The a-distribution is symmetric and shows an average major axis equal to column radius, while the b-distribution is skewed and shows a mean minor axis equal to half the column radius. The rising motions exhibit a variety of patterns, such as 2-D zigzag or swinging movements ($a \gg b$), 3-D spiral/rocking movements ($a > b$), or 3-D spiral movements ($a \approx b$). Figure 6b shows the distributions of the dimensionless distance d/R separating the ellipse centroid from the column centerline and of the inclination angle α of the ellipse defined as the angle between the ellipse major axis and x-axis. Regarding the flatness of the α-distribution, the multitude of spiraling paths the particle can take are all circumferentially equiprobable. However, there is a privileged radial range where the majority of the centroids lie. By evaluating the area under the curve, it is found that 90% of the centroids are between $d/R = 0$ and $d/R \approx 0.63$. Most of the ellipses are eccentric with respect to the column centerline (d/R from 0 to ≈ 0.1), which probably indicates that multiple bubble streams coexist simultaneously in the bed core region. Beyond $d/R \approx 0.63$ up to the column walls, incursions of the rising motion in the wall region are almost absent. Therefore, the previously mentioned clusters of bubbles or coalesced bubbles that are responsible for the particle rising movements occupy a preferential central region in the bed. This region coincides well with the central fast-bubble flow region, where similar qualitative behaviors of liquid and solids were observed by Chen et al. (1994). Henceforth, this region will be referred to as the *fast-bubble flow region*. It is worth mentioning that the outer radius $r/R = 0.63$ of this fast-bubble flow region is not arbitrarily set. It corresponds to the flow inversion line or the locus of the zero mean axial velocity of the solids (discussed later). This line roughly separates the core upward flow where the bubbles emerge the most and the flow along the sidewall, where the particles move predominantly downward. It is important to realize that the limits of the fast-bubble flow region are not sharp boundaries, since some rising movements, albeit negligible, can also be detected in the wall region (Figure 6a and 6b).

Particle Downward Movement. Thus far we have described the solids movements due to the wake upflow in the fast-bubble flow region. Now, we examine how the particle downward movements are affected once the particles are expelled toward the liquid–solid emulsion. The downward solids motion naturally arises as a response to counterbalance the ascend-

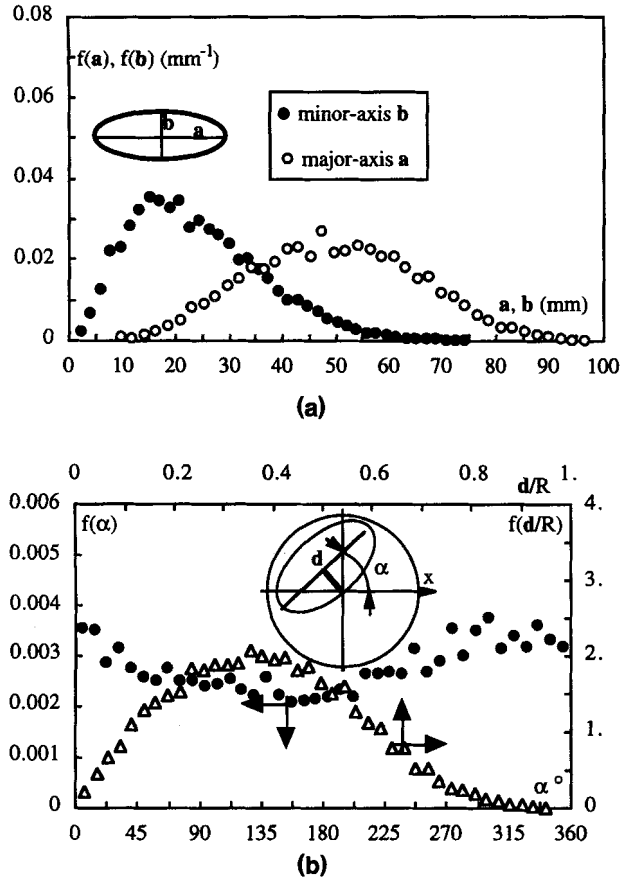

Figure 6. Normalized density functions of (a) the minor *a* and major *b* axes of the outermost ellipse enclosing the particle movement in the wakes; (b) the distance *d/R* separating the ellipse centroid from the column centerline and the inclination angle α of the major axis with respect to the x-axis.

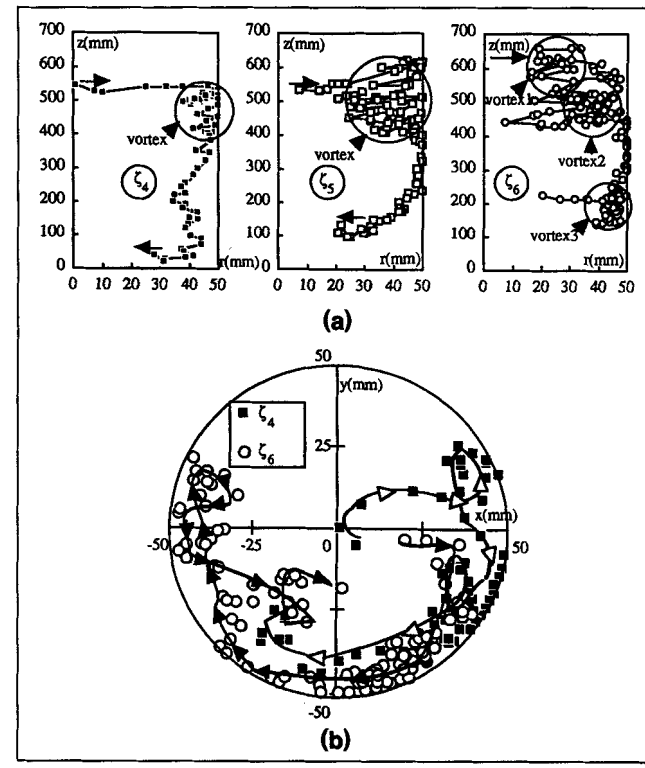

Figure 7. Typical features exhibited during particle descents (a) radial vs. axial displacements for the descending portions ζ_4, ζ_5, and ζ_6, and (b) cross-sectional movements for portions ζ_4 and ζ_6.

ing solids flow induced by rising bubbles in the fast-bubble flow region. As a result of these movements, a gross circulation structure of the solids is established in the bed.

Figure 7a shows r vs. z instantaneous motions of the tracer for the three descending paths labeled ζ_4, ζ_5, and ζ_6 in Figure 3a. The descending trajectories, where zigzag motions are now no longer observed, characteristically differ from the ascending movements of Figure 5a. Figure 7b is a top view of the horizontal projections of the trajectories corresponding to portions ζ_4 and ζ_6. The solid particles sink preferentially adjacent to the vessel walls. They descend diagonally with a slight lateral migration toward the center until they enter the neighboring fast-bubble flow region. From Figure 7a and 7b, it appears that the solids slide downward in a spiral manner between the wall and the fast-bubble flow region. This behavior is not exceptional and has been observed in most cases where the particles went down. In contrast with the rising spirals, the descending spirals never complete loops even though rising and descending velocities of the particles do not differ much (see below). The kinematic features associated with the downward motion clearly indicate that a second flow region exists with solids predominantly flowing downward in a spirallike motion. The existence of such a region has been directly shown by Chen et al. (1994) and Tzeng et al. (1993) to be located adjacent to the column wall and characterized by downward liquid and/or solids streams moving in either a straight or spiral manner, depending on the fluid throughputs. Henceforth in accordance with the nomenclature of Chen et al. (1994), we refer to this region as the descending flow region.

By constructing the radial distribution of radii where the particles start sinking in the liquid–solid emulsion, the horizontal width of the descending flow region can be estimated. Figure 8 shows such a distribution expressed in terms of dimensionless radius $\xi = r/R$. Here, $F(\xi)\Delta\xi$ represents the fraction of times the tracer goes down between radii ξ and $\xi + \Delta\xi$, regardless of axial position. As expected, there exists a privileged radial range where most downward movements take place. Although it may happen that the particles move downward in the central region, most of the solids downflow occurs between $\xi \approx 0.63$ and 1. As argued before for the fast-bubble flow region, the limit at $\xi = 0.63$ can be taken as a rough estimation of the radial separation between the fast-bubble flow region and the descending flow region.

Vortical Flow Region. A third motion mechanism is exhibited by the trajectory between the moment where the particle quits a bubble wake until the moment where it starts a descent. Figure 7a shows that the particle is first repelled out-

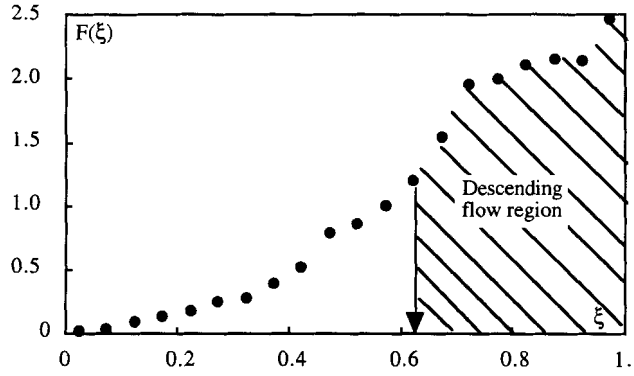

Figure 8. Normalized density function of the radial positions where the particle sinks toward the bottom; the dashed area show the descending flow region starting at $\xi = 0.63$.

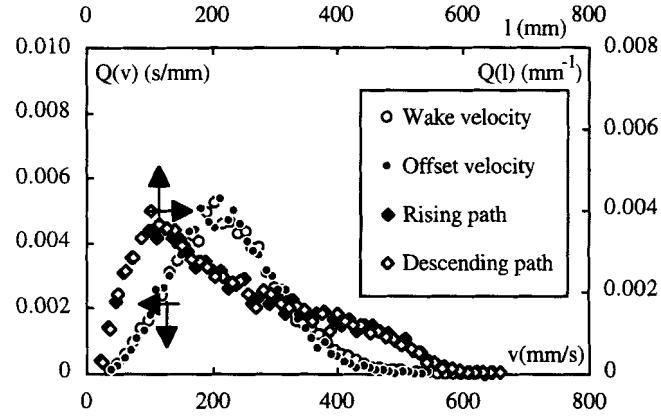

Figure 9. Wake and solids offset flow path and velocity distributions in the vortical-spiral flow regime.

ward from the fast-bubble flow region toward the wall region. Then the particle is entrained and remains entrapped for a while (from a few tenths of second to around one second) in a sidewall cell where its movement looks frenetic and untidy (Figure 7a). These cells form near the free bed surface, most often close to the wall, and are likely brought about by the secondary motion caused by the intense discharge of wake material near the freeboard. Similar sidewall cells are also observed in the longitudinal direction within the bed, for example, ζ_6 at $z \approx 460$ mm (vortex #2) and $z \approx 220$ mm (vortex #3) of Figure 7a. Apparently, these cells are akin to the liquid–solid vortices of the vortical flow region identified by Tzeng et al. (1993) and Chen et al. (1994), and which lie between the fast-bubble flow region and the descending flow region. Several representative samples, as those shown in Figure 7a, analyzed from the complete trajectory record indeed show that this third flow region is confined between the fast-bubble flow and the descending flow regions. As in Chen et al. (1994), we call this region the *vortical flow region*. Notice that because of the dynamic nature of the vortices that invade more or less the descending flow region, it is very difficult to draw sharp boundaries between the vortex region and the nearby descending flow region. We will see later how the contour plots of axial turbulence intensity and velocity fields of the time-averaged flow pattern help define more visibly the three previously mentioned regions.

Particle Velocity Distributions. The previous analysis of local displacement characteristics of the solids showed three types of motions, namely a bubblelike or wake motion in the fast-bubble region, a convective offset motion in the sidewall descending flow region, and a random motion in the vortical flow region. The two former are characterized by long-amplitude displacements and are responsible for the solids gulf stream or bed gross circulation, whereas the latter occurs mainly between the central upward stream and the annular descending stream in the liquid–solid emulsion. Based on this classification, distributions of the rising and descending paths and velocities of the solids can be determined. A rising (resp., descending) path is defined as the vertical distance crossed by the particle before it is deviated from its initial course by any disturbance. The rising (resp., descending) velocity is calculated from the rising (resp., descending) distance and elapsed time. Because of the short-range random displacements, a careful screening of the experimental data must be exercised. Thus, all events to which vertical amplitudes are less than 10 mm, or movements that do not keep rising or descending for more than five successive sampling periods (i.e., 0.15 s or less), are believed to belong to the random emulsion motion and have been discarded. The choice of threshold values of 10 mm or 0.15 s is not arbitrary, but has been set by a trial-and-error procedure until very high instantaneous velocities arising from the fluctuating displacements are sensitively reduced. Note that such threshold values mainly affect the extent of the tail of the velocity distributions and only slightly the average velocity.

Figure 9 shows rising (wake motion) and descending (offset motion) path and velocity distributions for the solids in the vortical spiral flow regime. Note that the particle velocity represents an absolute velocity with respect to a stationary frame, and that the path and velocity distributions given here are based on number frequencies. Both distributions are skewed and broad, but still remain unimodal as should be the case in the coalesced bubble flow regime (Matsuura and Fan, 1984). Interestingly, wake and offset distributions almost coincide. The mean free path is 230 mm and the mean particle velocity is 225 mm/s. Comparison with results obtained in the dispersed-bubble flow regime for the same 3-mm glass beads in binary mixtures with 5-mm glass beads or 5.5-mm polyvinylchloride particles showed qualitatively different trends between the rising and the descending distributions (Larachi et al., 1995). In the dispersed-bubble flow regime, the particles were found to move faster in the wakes than in the offset flow. As only a few experiments are available for the moment, it is difficult to draw conclusions on the repercussions of the flow regime on the velocity distributions. It seems, however, that the particle velocity distributions broaden and the mean velocities increase with increasing gas superficial velocity, which qualitatively agrees with some recent measurements on bubble rise velocities made by Yu and Kim (1988) and by Chen et al. (1995).

Mean flow pattern

So far the Lagrangian analysis demonstrated the complex

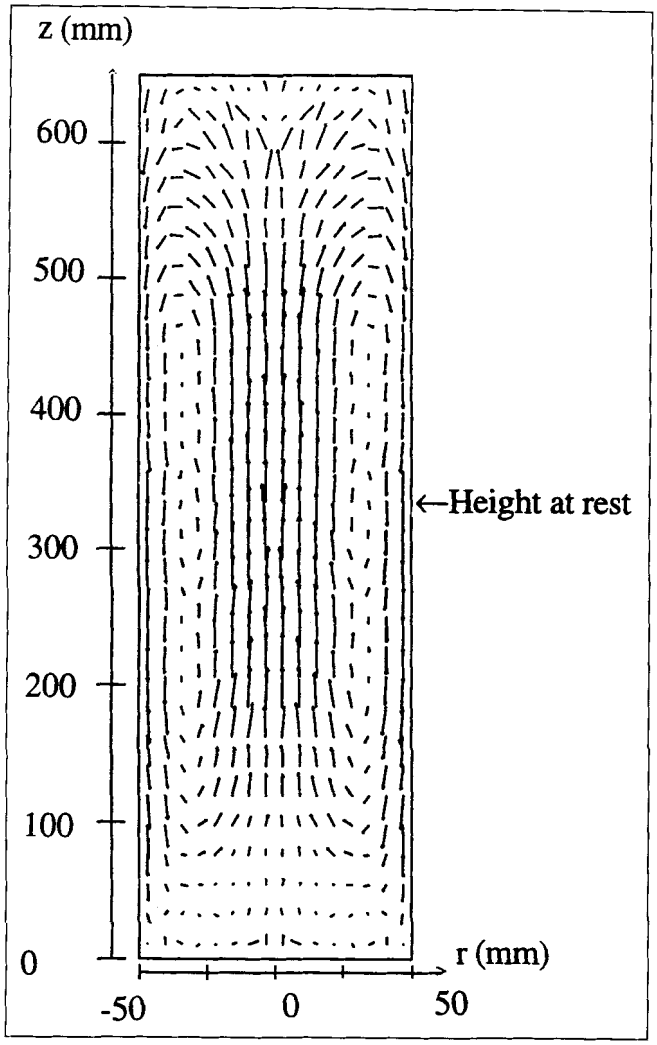

Figure 10. Circumferential and time-averaged recirculatory velocity field of the solids.

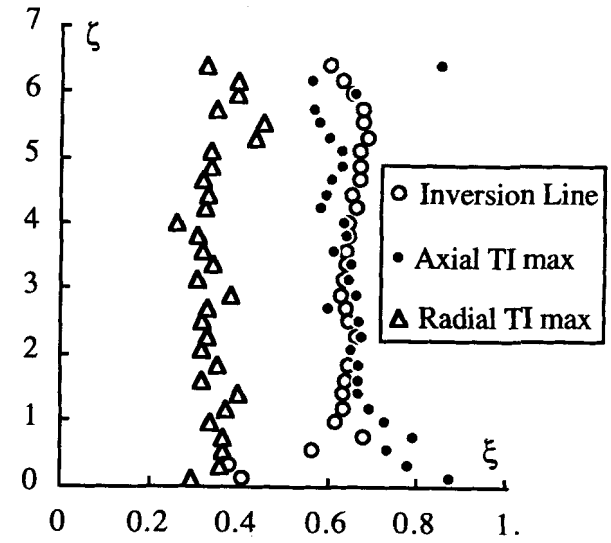

Figure 11. Loci of the solids flow inversion line, and of the maximum radial and axial turbulence intensity.

dynamic structure of the solids flow field in three-phase fluidized beds in the vortical-spiral flow regime. Various mechanisms have thus been shown to be responsible for the macroscopic solids movements. Quite often, flow-field descriptions in Lagrangian frames are qualitative and profuse, and seldom consent to synthetic representations. Thus, alternate but complementary descriptions using the Eulerian frame may prove useful for quantitatively representing the time-averaged behavior of the solids flow field and for diagnosing mean recirculatory patterns. Even though some inherent flow mechanisms may be lost in the averaging procedures (e.g., spirals during circumferential averaging), Eulerian descriptions are preferred because they are more tractable. Thus, the three-phase emulsion is purposely divided into 16 azimuthal slices of 8 radii and 30 axial cuts so that a grid of up to 4,000 compartments is generated.

An instantaneous Eulerian velocity is estimated by subtracting the coordinates of two successive position vectors and by dividing by the counting time interval. The resulting velocity is assigned to the center of the sampling compartment where the midpoint between the two subsequent positions falls. Within each compartment, an ensemble-averaged velocity and a root-mean-square velocity can be directly estimated by summing each velocity component and dividing by the total number of instantaneous velocities assigned to the compartment under consideration. Up to 4,000 events are accumulated per compartment over a 6-h experiment. However, as a result of the statistical nature inherent to nuclear decays, the γ-ray counts measured fluctuate, which implies that the calculated tracer coordinates are noisy. To obtain the true flow root-mean-square velocities, the spurious velocities arising from the γ-radiation fluctuations are subtracted in quadrature from the calculated root-mean-square velocities. The spurious velocities are estimated by using a space-resolution mapping established from the calibration procedure. Readers interested in more details on the velocity calibration and the evaluation of the 3-D resolutions are referred to the following papers (Larachi et al., 1994; Godfroy et al., 1995).

By assuming axisymmetry of the solids flow, the angular dimension is taken out by averaging azimuthally the ensemble-averaged velocities. After dropping the azimuthal dependence, one arrives at a 2-D velocity vector field of radial component, U_r, vs. axial component, U_z, which can be plotted as a plane vector. Local relative turbulence intensities defined as the ratio of the root-mean-square velocity and the maximum centerline axial velocity, respectively $I_z = u/U$ and $I_r = u/U$ for the axial and radial directions, are also obtained. It is clear that the pattern resulting after time and circumferential averaging does not fully represent the instantaneous features of the particle movements such as those of the vortical flow region, or those of the fast-bubble flow region. Nevertheless, 2-D r-z profiles ought to be very useful in providing synthetic data for modeling flows that are axisymmetric.

Figure 10 shows a typical example of the azimuthally and time-averaged solids Eulerian velocity field. The length of each velocity vector in the field is proportional to the local average particle speed, the arrowhead indicates the local mean direction of the flow of the solids, and the starting point

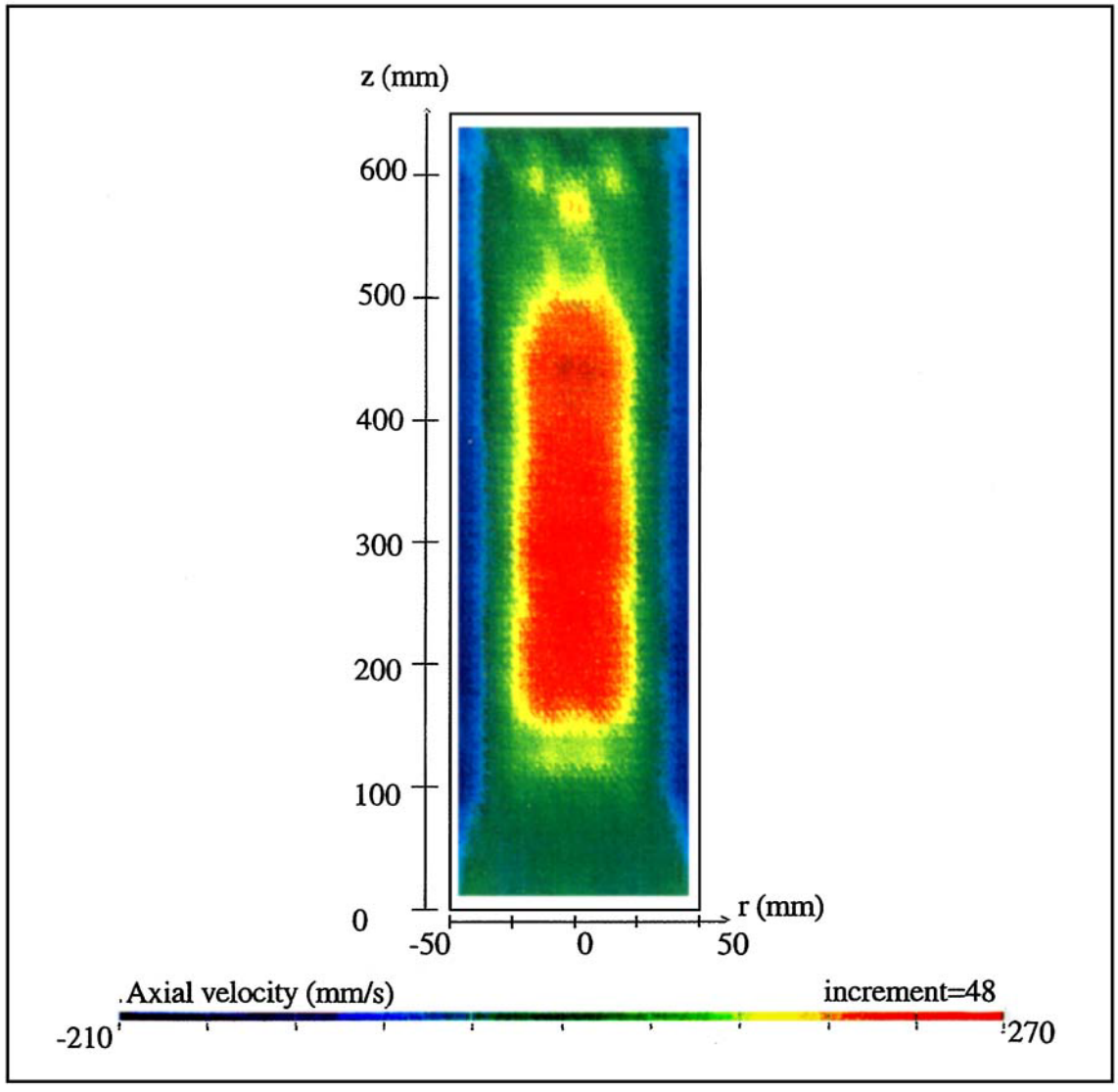

Figure 12a. Contour plots of the particle: axial velocity.

corresponds to the center of the sampling compartment. The bed height at rest is indicated with an arrow at $z = 330$ mm. It is observed that a pair of large toroidal recirculation cells fills the entire bed height. These cells rotate in a clockwise direction. The maximum speed induced by the gas flow is 267 mm/s and occurs in the column centerline. The locus of the zero axial velocity, that is, the inversion line, is plotted in Figure 11 as radial ($\xi = r/R$) vs. axial ($\zeta = z/D$) dimensionless coordinates. On an average basis, this inversion line separates the particle upflow central region (fast-bubble flow region) from the particle downflow sidewall region (descending flow region). For the conditions and bed material used in this study, the radial location of inversion changes from $\xi \approx 0.4$ to $\xi \approx 0.63$ up to a ζ ratio of 1.3 in the entrance region, then it stabilizes around $\xi \approx 0.63$ for the bulk region for a ζ in the range [1.3–5], and finally it slightly diminishes to 0.60 near the disengagement zone. The changes observed on the radial location of inversion in the bed entrance region are found to agree qualitatively with recent measurements made by Reese and Fan (1994) on the liquid flow in the entrance region of a bubble column. However, a value of $\xi \approx 0.7$ for the inversion point in the bulk region observed by most of the researchers in bubble columns (Devanathan et al., 1990; Gross and Kuhlman, 1992; Chen et al., 1994; Reese and Fan, 1994) is not confirmed in this study for the solids in three-phase fluidized bed.

The steady flow pattern of the solids in the recirculation cells of Figure 10 is consistent with that identified by Chen et al. (1994) for the liquid phase in both the bubble-column and low-solids holdup three-phase fluidized bed. Similar "gulf stream" patterns were also reported for the liquid in bubble columns (Hills, 1974; Franz et al., 1984; Devanathan et al., 1990; Reese and Fan, 1994), and for the solids in gas fluidized beds (Moslemian et al., 1989). The previously observed solids flow pattern has obvious implications on existing modeling procedures and current theories of flow behaviors. For instance, the pervasive axial dispersion model is clearly inadequate to describe only the convective pattern of solids evidenced by RPT.

To delineate the boundaries of the time-averaged flow structure of the solids, contour plots of the average axial velocity U_z, and radial and axial turbulence intensities, I_r and

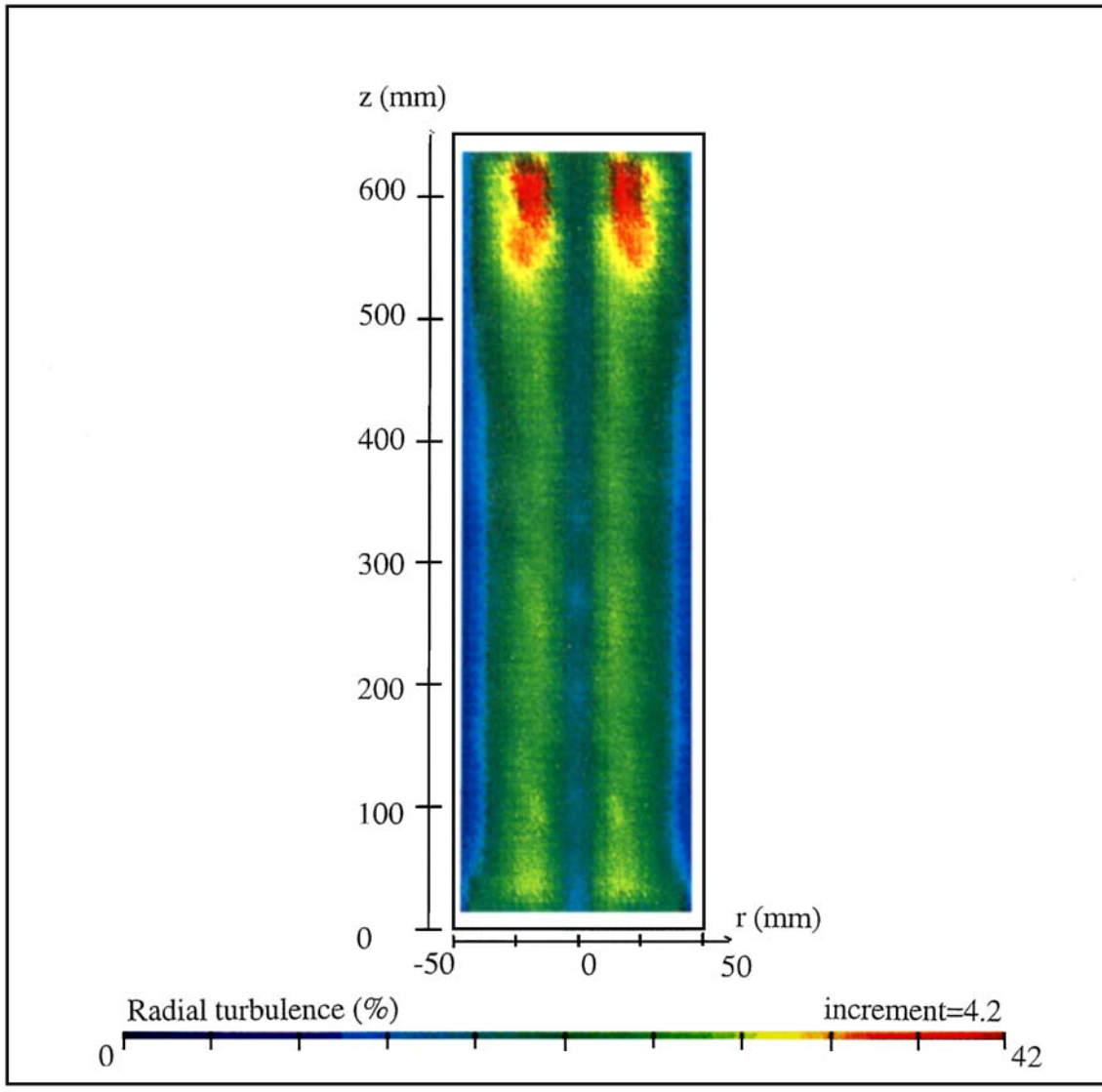

Figure 12b. Contour plots of the particle: radial turbulence intensity.

I_z, are drawn in Figures 12a–12c. Before proceeding further in the interpretation of these contour plots, one has to bear in mind that the results might not be valid for particles of different size and/or density, for which further work is needed.

The development of the axial particle velocity over the entire flow field in the vortical-spiral flow regime is illustrated by the contour plot of U_z in Figure 12a. In the figure one clearly distinguishes the descending flow region (negative velocities), the central fast-bubble flow region (positive velocities), and the flow inversion line (see also Figure 11). As seen, axial velocities approximately follow bell-shaped radial profiles. The solids upflow proceeds from an accelerating developing flow ($0 \le \zeta \le 1.3$) to a fully developed flow ($1.3 \le \zeta \le 5$), and then till the disengagement zone ($\zeta \ge 5$) to a decelerating flow. In the acceleration region, immediately above the distributor, the solids flow begins with nearly no convection velocity. Then quickly, a distinct downward flow, showing higher U_z magnitudes than the central flow, occurs close to the walls. Apparently, the wall flow in the acceleration region forces the gas bubbles evolving from the distributor to migrate toward the central region, where they progressively accelerate. However, being still tiny the bubbles cannot efficiently raise the solids. As they continue to rise, the bubbles coalesce to form bubbles that become large enough to carry particles up in their wakes. The outbreak of the fully developed region seen in Figure 12a qualitatively agrees with the axial location where wakes become active, as depicted in Figure 4. In the fully developed flow or bed bulk region, the radial profile of U_z is approximately parabolic and does not change appreciably with the vertical distance. The velocity distribution, and hence the size of the up and downflow regions, remains constant in the bulk region, which indicates that the average flow of the solids is one-dimensional. Furthermore, it is seen that the downward velocity (maximum 210 mm/s) of the descending flow region has a smaller value than the upward velocity (maximum 267 mm/s) of the fast-bubble flow region. A visible correspondence between the gas holdup profile and the axial solids velocity distribution should be expected. Further work to clarify this coupling is neces-

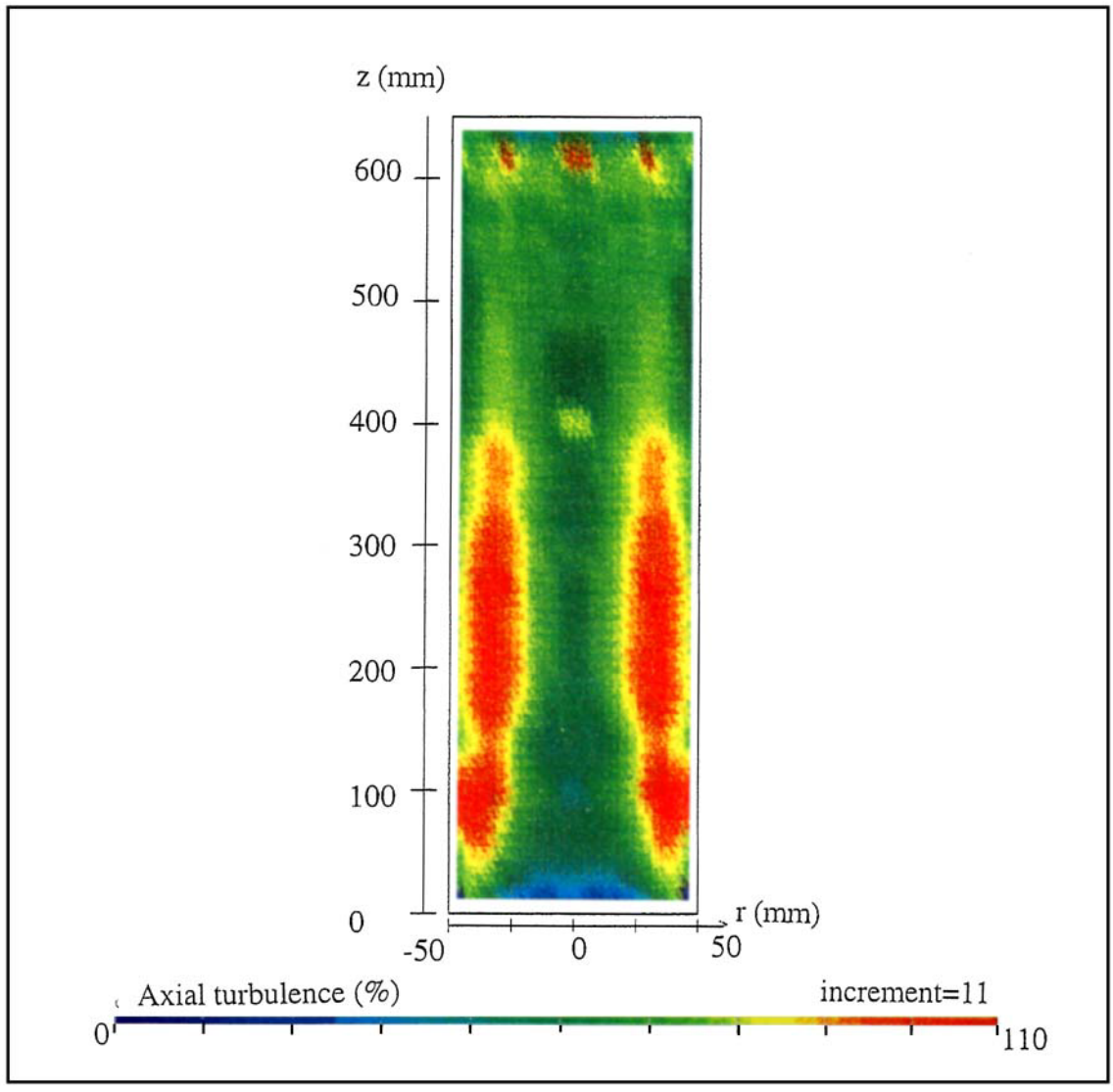

Figure 12c. Contour plots of the particle: axial turbulence intensity.

sary after simultaneous measurements on gas holdup and particle velocity distributions will be available.

The highest radial turbulence intensity occurs within the fast-bubble flow region, where the swinging and the spiral/rocking movements of the particles have been observed. The turbulence intensity I_r reaches a maximum at $\xi \approx 0.4$ (Figure 11), whereas it is minimal near the wall (Figure 12b), as it should be. It is within the deceleration region that I_r is the highest. There a significant fraction of the particle-rising kinetic energy is converted into radial turbulence kinetic energy as a consequence of the intense discharge of solids from bubble wakes (see also Figure 4). The contour plot of turbulence intensity I_z in Figure 12c shows the presence of an intermediate annular region, between the central fast-bubble flow and the wall regions, where longitudinal turbulence is the highest. Comparison between the geometrical locus where I_z is maximum and the locus where flow is reversed shows that the two lines roughly coincide (see Figure 11). The thickness of this region is irregular and varies with height. The region of maximum axial turbulence is seen to merge distinctly with the descending flow region of the sidewalls. This region definitely represents the vortical flow region identified earlier (Figure 7a).

In comparison to the relative turbulence intensities known from fluid single-phase pipe flows, the ones measured for the solids in gas–liquid–solid fluidization are of noticeably higher magnitudes. From Figures 12b and 12c, it may be noticed that at a given radial location the intensities of the radial and axial turbulence velocities differ appreciably from one another over the whole bed. Recall that local turbulence intensity is expressed with respect to the maximum centerline axial velocity. The turbulence intensity in the axial direction always has a higher value (up to 110%) than the intensity in the radial direction (up to 42%). Clearly, the condition of isotropy is not fulfilled anywhere in the reactor.

Some selected longitudinal distributions of the azimuthally and time-averaged radial velocity U_r and radial turbulence intensity I_r, and axial velocity U_z taken at four representative radial positions $\xi = 0.06$, 0.56, 0.69, and 0.81 are shown in Figures 13a–13c as a function of coordinate z. The axial par-

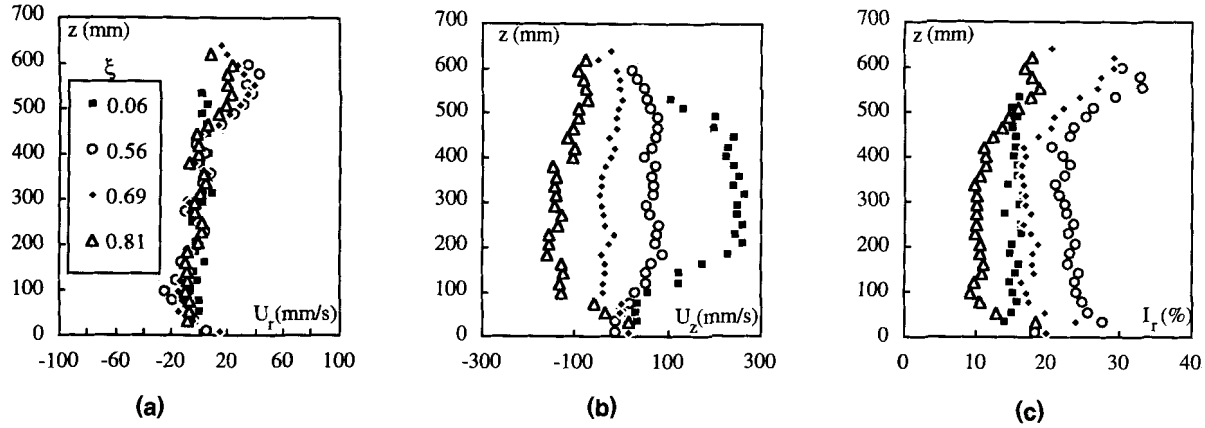

Figure 13. Selected longitudinal distributions of (a) radial and (b) axial mean velocities, and (c) radial turbulence intensities.

ticle velocity is largest at a fixed depth for a smaller radius, near the centerline; whereas at $\xi \approx 0.69$, it is close to zero due to the proximity with the inversion line. Throughout the major part of the column, the average radial velocities appear to go to zero as either the column wall or the centerline is approached. Overall, the mean radial velocity is small and inward (negative) for the lower part of the recirculation cell. However, the mean radial velocity is positive (outward) in the upper region of the bed. Moreover, mean radial velocities are consistently lower than the corresponding radial turbulence velocities (Figures 13a and 13c). For any given radial location, turbulence intensity I_r is a weak function of coordinate z, except for the decelerating region ($\zeta \geq 5$), where it is particularly high. Practically, this means that the statistical theory of homogeneous fields can provide a preliminary approach to modeling the particles radial motion.

Concluding Remarks

For the first time, the motion of the solids phase in a three-dimensional three-phase fluidized bed has been studied and related to the characteristics of the prevailing flow regime. This has been done with a radioactive particle tracking technique (RPT).

The present data with RPT extend the observations on the flow structure made on dilute and transparent three-phase systems by laser sheeting techniques (Chen et al., 1994) for the study and the understanding of the solids behavior in opaque and/or dense three-phase fluidized beds. Currently, new experiments are undertaken with different particle and liquid properties in order to assess the conceptual model for solids flow structure in 3-D three-phase fluidized bed proposed by Chen et al. (1994).

It is observed that the high level of mixing of the bed particles is mainly triggered by large-scale vertical movements brought about by the bubbles that carry particles in their wake regions. In addition, the bubble wakes are nonisolated in that solids are thrown not only into the disengagement region but also along the bed height into the emulsion. The velocity distributions of rising and descending particle paths are found not to differ appreciably.

The RPT data have also been used to sketch the flow structure of the solids in the vortical-spiral flow regime. Three flow regions are identified and are here listed in increasing order of radial positions:

- A fast-bubble flow region preferentially forms a core region for $0 \leq r/R \leq 0.63$, where the wake motion associated with large coalesced bubbles is responsible for the rising swirling movements of the particles.
- An annular descending flow region adjacent to the column wall and the fast-bubble flow region forms between $r/R = 0.63$ and 1, and where particles circulate downward in a spiral manner.
- An annular vortical flow region adjacent to the fast-bubble flow region and often merging with the descending flow region, forms due to the formation of emulsion vortices where the captured particles execute frenetic looping patterns. This region roughly encloses the line where the average vertical flow of particles is reversed or where longitudinal turbulence intensity is maximum.

The RPT experiments demonstrated the existence of a stationary gulf stream for the solids composed of a pair of toroidal recirculatory cells. This observation invalidates pervasive uses of axial dispersion models to describe the solids movements in gas–liquid–solid fluidization.

Acknowledgments

The authors wish to acknowledge the assistance of Dr. G. Kennedy and Mr. Saint-Pierre of the Energy Engineering Institute of École Polytechnique. Financial support from the Natural Sciences and Engineering Research Council and the Fonds pour la Formation de Chercheurs et l'Aide à la Recherche du Québec are also gratefully acknowledged.

Notation

D = column diameter, mm
f = density function of the ellipse characteristic measures
F = density function of radial positions where the particle starts descending
l = path length, mm
N_0 = total number of sheddings
Q = density function of the wake and offset particle path and velocity

r = radial position, mm
R = column radius, mm
u' = azimuthally and time-averaged Eulerian root-mean-square particle velocity, mm/s
v = absolute particle rising or descending velocity, mm/s
W = wake–emulsion solids exchange distribution, mm^{-1}

Literature Cited

Cassanello, M., F. Larachi, M.-N. Marie, C. Guy, and J. Chaouki, "Experimental Characterization of the Solid Phase Chaotic Dynamics in Three-Phase Fluidization," *Ind. Eng. Chem. Res.*, **34**, 2979 (1995).

Cassanello, M., F. Larachi, C. Guy, and J. Chaouki, "Solids Mixing in Gas-Liquid-Solid Fluidized Beds: Experiments and Modeling," *Chem. Eng. Sci.*, **51**, 2011 (1996).

Chen, R. C., and L.-S. Fan, "Particle Image Velocimetry for Characterizing the Flow Structure in Three-Dimensional Gas-Liquid-Solid Fluidized Beds," *Chem. Eng. Sci.*, **47**, 3615 (1992).

Chen, R. C., J. Reese, and L. S. Fan, "Flow Structure in a Three-dimensional Bubble Column and Three-phase Fluidized Bed," *AIChE J.*, **40**, 1093 (1994).

Chen, Z., C. Zheng, Y. Feng, and H. Hofmann, "Modeling of Three-Phase Fluidized Beds Based on Local Bubble Characteristics Measurements," *Chem. Eng. Sci.*, **50**, 231 (1995).

Devanathan, N., D. Moslemian, and M. P. Dudukovič, "Flow Mapping in Bubble Columns using CARPT," *Chem. Eng. Sci.*, **45**, 2285 (1990).

Dudukovič, M. P., N. Devanathan, and R. Holub, "Multiphase Reactors: Models and Experimental Verification," *Rev. Inst. Fr. Pétr.*, **46**, 439 (1991).

Dudukovič, M. P., and N. Devanathan, "Bubble Column Reactors: Some Recent Developments," *Chemical Reactor Technology for Environmentally Safe Reactors and Products*, NATO ASI Ser. E: Appl. Sciences, H. I. de Lasa, G. Dou and A. Ravella, eds., p. 353 (1993).

Fan, L.-S., *Gas-Liquid-Solid Fluidization Engineering*, Butterworth Series in Chemical Engineering, Stoneham, MA (1989).

Fan, L.-S., J. W. Tzeng, and H. T. Bi, "Flow Structure in a Two-Dimensional Bubble Column and Three-Phase Fluidized Bed," *Fluidization*, Vol. III, O. E. Potter and D. J. Nicklin, eds., Engineering Foundation, New York, p. 399 (1992).

Franz, K., T. Börner, H. J. Kantorek, and R. Buchholz, "Flow Structure in Bubble Columns," *Ger. Chem. Eng.*, **7**, 365 (1984).

Godfroy, L., F. Larachi, G. Kennedy, B. P. A. Grandjean, and J. Chaouki, "On-Line Flow Visualization in Multiphase Reactors using Neural Networks," *Appl. Radiat. Isot.*, (1995).

Gross, R. W., and J. M. Kuhlman, "Three-Component Velocity Measurements in a Turbulent Recirculating Bubble-Driven Liquid Flow," *Int. J. Multiphase Flow*, **18**, 413 (1992).

Hills, J. H., "Radial Non-Uniformity of Velocity and Voidage in a Bubble Column," *Trans. Ind. Chem. Eng.*, **52**, 1 (1974).

Kitano, K., and L.-S. Fan, "Near-Wake Structure of a Single Gas Bubble in a Two-Dimensional Liquid-Solid Fluidized Bed: Solids Holdup," *Chem. Eng. Sci.*, **43**, 1355 (1988).

Kreischer, B. K., H. Moritomi, and L.-S. Fan, "Wake Solids Holdup Characteristics behind a Single Bubble in a Three-Dimensional Liquid-Solid Fluidized Bed," *Int. J. Multiphase Flow*, **16**, 187 (1990).

Larachi, F., G. Kennedy, and J. Chaouki, "A γ-Ray Detection System for 3-D Particle Tracking in Multiphase Reactors," *Nucl. Instr. Meth.*, **A338**, 568 (1994).

Larachi, F., M. Cassanello, M.-N. Marie, J. Chaouki, and C. Guy, "Solids Circulation Patterns in Three-Phase Fluidized Beds Containing Binary Mixtures of Particles as Inferred from RPT," *Trans. Ind. Chem. Eng.*, **73**, 263 (1995).

Lin, J. S., M. M. Chen, and B. T. Chao, "A Novel Radioactive Particle Tracking Facility for Measurement of Solids Motion in Gas Fluidized Beds," *AIChE J.*, **31**, 465 (1985).

Matsuura, A., and L.-S. Fan, "Distribution of Bubble Properties in a Gas-Liquid-Solid Fluidized Bed," *AIChE J.*, **30**, 894 (1984).

Miyahara, T., K. Tsuchiya, and L.-S. Fan, "Mechanism of Particle Entrainment in a Gas-Liquid-Solid Fluidized Bed," *AIChE J.*, **35**, 1195 (1989).

Miyahara, T., K. Tsuchiya, and L.-S. Fan, "Effect of Turbulent Wake on Bubble-Bubble Interaction in a Gas-Liquid-Solid Fluidized Bed," *Chem. Eng. Sci.*, **46**, 2368 (1991).

Moslemian, D., M. M. Chen, and B. T. Chao, "Experimental and Numerical Investigations of Solids Mixing in a Gas-Solid Fluidized Bed," *Particulate Sci. Technol.*, **7**, 335 (1989).

Moslemian, D., N. Devanathan, and M. P. Dudukovi, "Radioactive Particle Tracking for Investigation of Phase Recirculation and Turbulence in Multiphase Systems," *Rev. Sci. Instrum.*, **63**, 4361 (1992).

Reese, J., and L.-S. Fan, "Transient Flow Structure in the Entrance Region of a Bubble Column using Particle Image Velocimetry," *Chem. Eng. Sci.*, **49**, 5623 (1994).

Sokolichin, A., and G. Eigenberger, "Gas-Liquid Flow in Bubble Columns and Loop Reactors: Part I. Detailed Modelling and Numerical Simulation," *Chem. Eng. Sci.*, **49**, 5735 (1994).

Tsuchiya, K., and L.-S. Fan, "Near-Wake Structure of a Single Gas Bubble in a Two-Dimensional Liquid-Solid Fluidized Bed: Vortex Shedding and Wake Size Variation," *Chem. Eng. Sci.*, **43**, 1167 (1988).

Tsuchiya, K., G. H. Song, W. T. Tank, and L.-S. Fan, "Particle Drift Induced by a Bubble in a Liquid-Solid Fluidized Bed with Low-Density Particles," *AIChE J.*, **38**, 1847 (1992).

Tzeng, J. W., R. C. Chen, and L.-S. Fan, "Visualization of Flow Characteristics in a 2-D Bubble Column and Three-Phase Fluidized Bed," *AIChE J.*, **39**, 733 (1993).

Yang, Y. B., N. Devanathan, and M. P. Dudukovi, "Liquid Backmixing in Bubble Columns via Computer Automated Particle Tracking (CARPT), *Chem. Eng. Sci.*, **47**, 2859 (1992); also *Exp. Fluids*, **16**, 1 (1993).

Yu, Y. H., and S. D. Kim, "Bubble Characteristics in the Radial Direction of Three-Phase Fluidized Beds," *AIChE J.*, **34**, 2069 (1988).

Manuscript received Sept. 12, 1994, and revision received Jan. 29, 1996.